ACS APPLIED MATERIALS & INTERFACES

Research Article

www.acsami.org

Hybrid Sensor Using Gold Nanoparticles and Conjugated Polyelectrolytes for Studying Sequence Rule in Protein–DNA Interactions

Steven Lukman,[†] Khin Moh Moh Aung,[†] Jie Liu,[‡] Bin Liu,*[,†,‡] and Xiaodi Su*[,†]

[†]Institute of Materials Research and Engineering, Agency for Science, Technology and Research (A*STAR), Singapore

[‡]Department of Chemical & Biomolecular Engineering, National University of Singapore, 4 Engineering Drive 4, Singapore 117576

Supporting Information

ABSTRACT: Protein–DNA interactions play center roles in many biological processes. Studying sequence specific protein–DNA interactions and revealing sequence rules require sensitive and quantitative methodologies that are capable of capturing subtle affinity difference with high accuracy and in a high throughput manner. In this study, double stranded DNA-conjugated gold nanoparticles (dsDNA-AuNPs) and water-soluble conjugated polyelectrolytes (CPEs) are used as cooperative sensing elements to construct a suit of hybrid sensors for detecting protein–DNA interactions, exploiting the differential Förster resonance energy transfer (FRET) with and without protein binding. Through a proper selection of CPEs in terms of charge properties relative to the charge of dsDNA-AuNPs and emission wavelengths relative to the AuNP extinction peak, the hybrid sensors can be constructed into "light-on", "light-off", and "two-way" models. Protein binding can be detected by fluorescence recovery, fluorescence quenching, or both ways, respectively. The "two-way" sensor allows for detection of proteins of any charge properties or unknown charge properties. With estrogen receptor (ERα and ERβ), their consensus DNA (5′-GGTCAnnnTGACC-5′) element, and all 15 possible singly mutated elements (i.e., 3 possible base substitutions at each of 1 to 5 positions from left to right of the 5′ end half site, GGTCA), we have demonstrated the accuracy of the hybrids sensors for determination of binding affinity constant, binding stoichiometry, and site- and nucleotide-specific binding energy matrix. The in vitro binding energy determined by the hybrid sensors correlates very well with the energy matrix computed from in vivo genome-wide ERα binding data using Thermodynamic Modeling of ChIP-Seq (rank correlation coefficient 0.98). The high degree of correlation of the in vitro energy matrix versus the in vivo matrix renders the new method a highly reliable alternative for understanding in vivo protein binding in the whole genome.

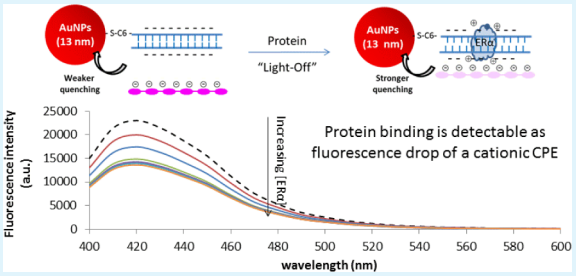

KEYWORDS: *gold nanoparticles, water-soluble conjugated polyelectrolytes, transcription factors, protein–DNA interactions, Förster resonance energy transfer, nanoparticle surface energy transfer*

1. INTRODUCTION

Metal nanoparticles and water-soluble conjugated polyelectrolytes (CPEs) are important materials in biomedical research because of their unique optical and electrical properties.[1−5] In the field of biosensing and bioanalytical chemistry, metal nanoparticles can support colorimetric detections exploiting the excitation of localized surface plasmon resonance and the interparticle distance-determined plasmonic coupling.[1,2] Metal nanoparticles can also support fluorimetric detections because of their ability to influence (quenching or enhancing) the emission of proximate fluorophores. The confinement of the surface plasmon resonance to the nanoparticle dimensions can either increase or decrease the amplitude of electromagnetic wave by as much as orders of magnitude, depending on the size and shape of the nanoparticles.[6−10] Fluorescence quenching-based bioassays with smaller size gold nanoparticles (AuNPs, <50 nm) have been developed in conjunction with various fluorophores, e.g., organic dyes,[11−15] quantum dots (QDs),[16−21] metal nanocluster,[22] green fluorescent proteins,[23] and water-soluble CPEs.[24−26]

Water-soluble CPEs, as (bio)sensing materials, have a better competitive edge than other luminescent materials because of their excellent light-harvesting capability, high quantum yield, and unique chain conformation.[3,4] Following the earlier discover of the super quenching of CPEs by AuNP made by Fan et al.,[27] coupling CPEs' excellent photon harvesting property with high extinction coefficient AuNPs has led to a number of biosensors exploiting versatile sensing principles.[6,23−26] For example, a handful of cationic AuNPs and anionic CPEs (ACPEs) have been used to form fluorimetric chemical nose/tongue for differentiating specific proteins, pathogen or cells.[24−26] Initially, the fluorescence of the

Received: September 21, 2013
Accepted: November 12, 2013
Published: November 12, 2013

ACPEs in the electrostatically complementary AuNP-CPE complexes is quenched. Addition of negatively charged analytes (proteins or cells) disrupts the AuNP-CPE complexes, resulting in fluorescence recovery. Differing from this example that uses direct Förster resonance energy transfer (FRET) and/or nanoparticle surface energy transfer (NSET) between metal nanoparticles and CPEs, silver nanoparticles (AgNPs, 40 nm) have been coupled with a cationic CPE (CCPE)-organic dye based FRET for DNA detection exploiting AgNPs enhanced fluorescence emission.[7] Xu's group has conducted comprehensive studies on AuNPs and AgNPs for their particle size dependent fluorescent quenching and enhancement to a range of CPEs.[9,10] In addition to FRET-based principle, Xia et al.[28] used CCPEs and their affinity to single-stranded DNA (ssDNA) to detect the complementary DNA and ssDNA binding analytes, because CCPEs specifically disrupt ssDNA's protection of AuNPs from aggregation.

In this study, we further harness water-soluble CPEs' unique optical and charge properties, as well as the prominent property of smaller AuNPs (13 nm) as a super fluorescence quencher, to develop a suit of hybrid sensors for studying sequence specific protein−DNA interactions, exemplified by two transcription factors (TFs), i.e., ER α and ERβ (estrogen receptor α and β). Five water-soluble CPEs of different emission wavelengths (from 410 to 630 nm) and charge properties (cationic and anionic) have been chosen. For the first time, their interactions with 13 nm AuNPs and double-stranded DNA (dsDNA)-conjugated AuNPs are studied. The detection of protein binding to DNA is based on the differential CPEs emission in DNA-coated AuNPs with and without protein binding. Depending on the choice of CPEs in terms of charge property relative to DNA and emission wavelength relative to AuNPs' absorption peak, the hybrid sensors have been constituted into "light-on", "light-off", or "two-way" models for detecting proteins of known and unknown charge properties, which is not always feasible with FRET assays using other donor−acceptor pair.[29]

Estrogen receptors play critical roles in regulating genes responsible for development and maintenance of reproductive tissues and other physiological function. The interaction of ERs with DNA sequences, known as estrogen response elements (EREs) (a palindromic repeat separated by three-base spacer, 5′GGTCAnnnTGACC-3′) is required for estrogen regulation of target gene expression.[30] In this study, we demonstrate that the hybrid sensors can differentiate the distinct binding affinity of two ER subtypes (ERα and ERβ) that have 96% similarity in their DBD (DNA binding domain), yet substantially different tissue distribution and function. For ERα, we further demonstrate that the hybrid sensors are highly sensitive to detect site- and nucleotide-specific single base variation impact on ERα binding affinity. With a total of 15 singly mutated EREs, each of them carrying one base variation in the 5′ end half-site with all possible base substitutions at each of the five possible sites, the hybrid sensors generate an in vitro binding energy model that correlates to an in vivo energy model determined by Thermodynamic Modeling of ChIP-seq (TherMos) with a higher accuracy than that generated by a sophisticated equipment (dual polarization interferometry) based in vitro model.[30] The high accuracy renders the hybrid sensor highly reliable in understanding of in vivo ERα binding in the whole genome.

Compared to previous AuNP-based colorimetric protein−DNA sensors using bare AuNPs[31] or two sets of dsDNA-conjugated AuNPs,[32,33] coupling salt screening,[34] or enzymatic cleavage of interparticle dsDNA linkages,[33] the current fluorimetric hybrid sensors overcome the limitations of (1) nonspecific aggregation of bare particles, (2) inadequate sensitivity to differentiate subtle affinity difference induced by single nucleotide variation,[31] (3) slow response in relation to the cleavage of DNA linkers inside the cross-linked AuNPs network,[32] and (4) extensive optimization of enzymatic reaction conditions[33] (enzymatic reaction is very sensitive to temperature and ionic strength of the liquid medium). In addition, with a competition assay approach, we can use the hybrid sensors to assess a large number of DNA sequences using only one set of dsDNA-AuNP conjugates.

2. EXPERIMENTAL SECTION

2.1. Materials. $HAuCl_4 \cdot 3H_2O$ (99.99%) and trisodium citrate dihydrate (99.9%) were obtained from Aldrich Pte Ltd. Purified recombinant human estrogen receptor (ERα and ERβ) was purchased from PanVera (Madison, WI, USA). They were stocked in HEPES buffer containing 10% glycerol. The stock concentration is 2800 nM for ERα and 4500 nM for ERβ. For long-term storage, the proteins were kept as 10 μL aliquots at −80 °C. Before use, they were thawed in room temperature water bath and returned to 4 C to maintain the activity.

A total of 17 EREs (35 bps: 1 wild type ERE "wtERE", 1 scrambled ERE "scrERE", 15 singly mutated EREs "mut1" to "mut15") were synthesized by Sigma Life Science. The sense sequences and their descriptors are given in Table 1. The wtERE contains perfect core sequence, 5′-GGTCAnnnTGACC-3′, and scrERE has both the 5′ and 3′ half-sites completely scrambled. The thiolated version of this sequence is denoted as thiol-wtERE and thiol-scrERE, respectively. The thiolated strands are conjugated to AuNP. In the 15 singly mutated sequences (mut1 to mut15), each has a base substitution at each of the 5 position in the 5′ end half-site with all possible substitutions. The sense strands and the antisense strands were annealed in phosphate buffered saline (PBS, pH 7.4) and stored at −20 °C.

Table 1. ERE Sequences

ID	sequence
wtERE	5′-AGTAAGCT cca**GGTCA** TTA **TGACC**tgg AGCTTACT− 3′
mut1	5′-AGTAAGCT cca***T***GTCA TTA **TGACC**tgg AGCTTACT-3′
mut2	5′-AGTAAGCT cca***C***GTCA TTA **TGACC**tgg AGCTTACT-3′
mut3	5′ −AGTAAGCT cca***A***GTCA TTA **TGACC**tgg AGCTTACT−3′
mut4	5′-AGTAAGCT cca**G*T*TCA** TTA **TGACC**tgg AGCTTACT-3′
mut5	5′-AGTAAGCT cca**GCTCA** TTA **TGACC**tgg AGCTTACT-3′
mut6	5′ −AGTAAGCT cca**GATCA** TTA **TGACC**tgg AGCTTACT−3′
mut7	5′-AGTAAGCT cca**GGGCA** TTA **TGACC**tgg AGCTTACT− 3′
mut8	5′-AGTAAGCT cca**GGCCA** TTA **TGACC**tgg AGCTTACT− 3′
mut9	5′-AGTAAGCT cca**GGACA** TTA **TGACC**tgg AGCTTACT− 3′
mut10	5′-AGTAAGCT cca**GGTGA** TTA **TGACC**tgg AGCTTACT-3′
mut11	5′-AGTAAGCT cca**GGTTA** TTA **TGACC**tgg AGCTTACT-3′
mut12	5′-AGTAAGCT cca**GGTAA** TTA **TGACC**tgg AGCTTACT-3′
mut13	5′-AGTAAGCT cca**GGTCG** TTA **TGACC**tgg AGCTTACT-3′
mut14	5′-AGTAAGCT cca**GGTC*T*** TTA **TGACC**tgg AGCTTACT-3′
mut15	5′-AGTAAGCT cca**GGTCC** TTA **TGACC**tgg AGCTTACT-3′
scrERE	5′-AGTAAGCT cca***TAGCG*** TTA ***CGCTA***tgg AGCTTACT-3′

Five water-soluble CPEs were utilized, including two anionic CPEs (ACPEs), i.e., poly[9,9-bis(4-sulfonatobutyl)fluorene-*alt-co*-1,4-phenylene] sodium salt (PFP-SO_3Na) and poly[5-methoxy-2-(3-sulfopropoxy)-1,4-phenylenevinylene] potassium salt solution and three cationic CPEs (CCPEs), i.e., poly[(2,5-bis(2-(*N*,*N*-

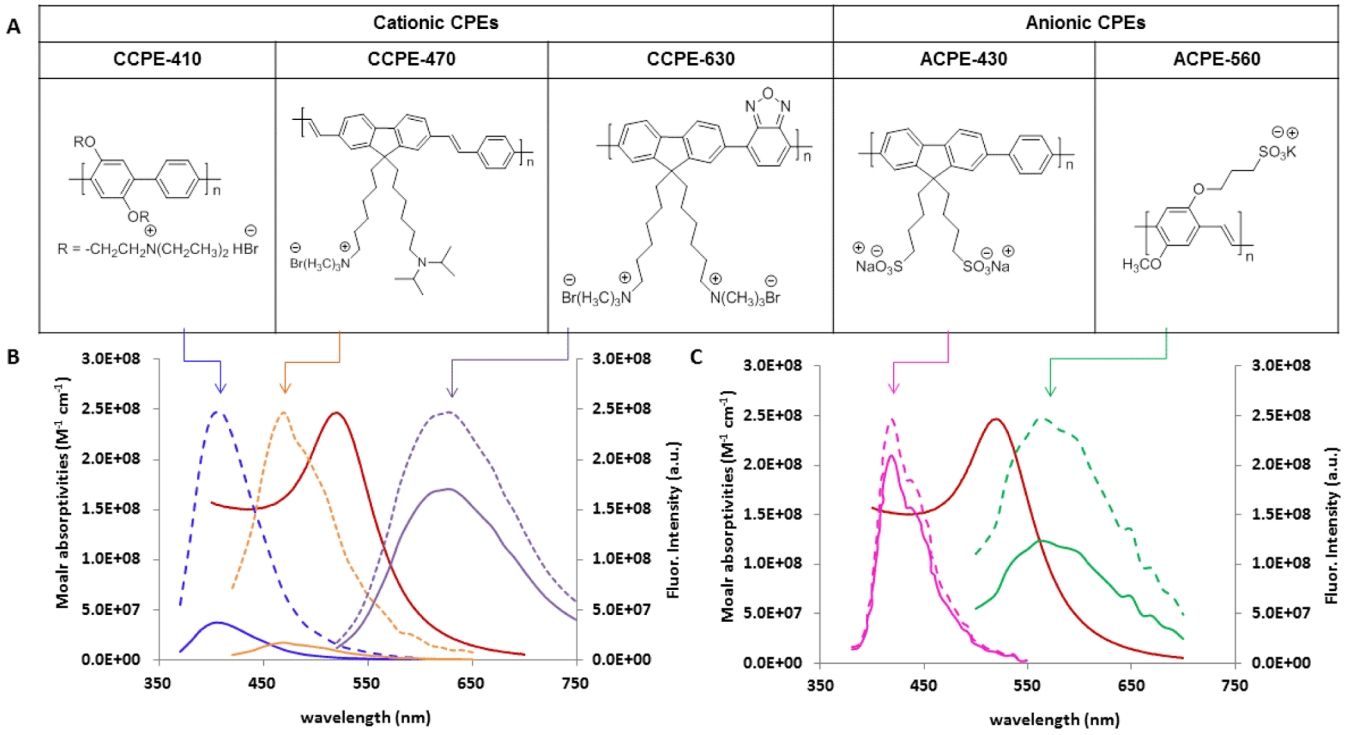

Figure 1. (A) Chemical structures of three CCPEs and two ACPEs used in this study. (B) CCPEs and (C) ACPEs emission spectra (dashed lines) and their quenched spectra (solid lines) in the presence of dsDNA-AuNP conjugates. AuNP's extinction spectrum (red) is shown as reference to indicate the spectral overlap.

diethylammoniumbromide)ethoxy)-1,4-phenylene)-*alt*-1,4-phenylene], poly[(9-(6-*N*,*N*,*N*-trimethylammonium)hexyl-9′-(6-*N*,*N*-diisopropylamine)hexyl)fluorenyldivinylene-*alt*-*co*-1,4-phenylene bromide] (PFVP) and poly[9,9-bis((6-*N*,*N*,*N*-trimethylammonium)-hexyl)fluorene-*alt*-*co*-2,1,3-benzoxadiazole dibromide] (PFBD). Their chemical structures are given in Figure 1A. According to their charge and the peak emission wavelength, they are denoted as ACPE-430, ACPE-560, CCPE-410, CCPE-470, and CCPE-630, respectively. The ACPE-560 and CCPE-410 were purchased from Sigma Aldrich, while the rest were synthesized in our lab.[29,34] The ACPE-430 and CCPE-470 have been previously used for detecting lysozyme[29] and single nucleotide polymorphism,[34] respectively. The CCPE-630 is yet published for its synthesis and application.

2.2. Synthesis of 13 nm AuNPs. AuNPs were synthesized via citrate reduction method, following the procedures available elsewhere.[31] The resulting AuNPs is approximately 13 nm in diameter and in a concentration of 5.33 nM, calculated according to Beer's law, using the extinction coefficient of 2.467×10^8 M^{-1} cm^{-1} for 13 nm AuNPs.

2.3. Preparation of ds-DNA Conjugated AuNPs. Thiolated single-stranded DNA (ssDNA) was activated with tris(2-carboxyethyl)phosphine) (TCEP, 10 molar excess) and stirred for 10 min. The final solution was centrifuged, with a Sigma-Aldrich microcon centrifugal filter device, YM-3 (NMWCO 3 kDa), to remove TCEP before conjugation to AuNPs. Conjugation of activated thiolated DNA to AuNP was done as described by Zhang et al.[35] Activated DNA was mixed with AuNPs at desired ratio (100:1) and incubated for 5 min. Then, pH of solution was lowered to 3 and salt concentration was increased to 30 mM by adding HCl and NaCl, respectively. After 20 min, NaOH was added to return pH to neutral range. This method took a shorter time of about 30 min to complete the DNA-AuNP conjugation. The ssDNA-AuNP conjugates were then annealed with its complementary DNA at 90 °C for 5 min and cooled to room temperature (RT). The amount of bound dsDNA was quantified after removing the unbound DNA via centrifugation (details in the Supporting Information, Figure S1). The dsDNA-AuNP entity is kept in the fridge (4 °C) for several weeks without appearance of any precipitation. The stability of AuNPs after DNA conjugation was tested using high salt solution (see the Supporting Information, Figures S2 and S3). The hydrodynamic size of the AuNPs before and after conjugation with dsDNA was measured with Dynamic Light Scattering System (BI-200SM, Brookhaven Instruments Corporation).

2.4. Fluorimetric Detection of Protein–DNA Binding Using AuNP/CPE Hybrid Sensors. The protein–DNA binding assay was conducted in three main steps. First, 50 nM of dsDNA-AuNPs was incubated with ER for 20–40 min at RT, in 10 mM PBS buffer (2.7 mM KCl and 137 mM NaCl, pH 7.4). For determination of the binding constant, K_d, and the stoichiometry, n, protein titration was conducted with increasing concentration from 0 to 250 nM. Second, CPE of 100 nM (i.e., 2:1 molar ratio to dsDNA-AuNP) was added to the dsDNA-AuNPs/protein mixture and incubated for an additional 10 min to let the system to reach equilibrium. Finally, the fluorescence spectra of the final solution were measured and compared with and without any protein. In control experiments of testing CPE's emission in the presence of DNA or protein without AuNPs, 50 nM of dsDNA or 250 nM protein was added into 100 nM CPEs in PBS buffer.

For screening relative affinity of ER to large number of mutant EREs, a competition assay is used with only one set of wtERE-conjugated AuNPs, but there was no need to prepare AuNPs conjugates for all EREs to be studied. Particularly, 3-fold of competitor ERE (mutated ERE) was incubated with the protein for 20–30 min prior to incubation with the wtERE-AuNP. The rest of the steps were the same as above.

3. RESULTS AND DISCUSSION

3.1. Characterization of dsDNA-Coated AuNPs. Water-soluble cationic CPEs and dsDNA-modified gold nanoparticles (dsDNA-AuNP) are the key sensing elements to construct the hybrid sensors. We first characterized the 35 bp wtERE-conjugated AuNPs in terms of surface charge, DNA coverage, hydrodynamic size (Table 2) that are essential for studying CPEs' interactions with dsDNA-AuNPs and the initial quenching. The hydrodynamic size expansion of 23.8 nm

Table 2. Characteristics of 35 bp wt ERE Conjugated AuNPs

particle measured	hydrodynamic diameter (nm)[a]	zeta potential (mV)	surface coverage (molar ratio)[b]
bare AuNPs	20.4 ± 2.18	−39.2 ± 3.5	N.A.
wtERE-AuNPs	44.2 ± 2.16	−32.6 ± 3.4	89.6 ± 5.3

[a]Measured by dynamic light scattering. [b]Molar ratio of dsDNAs that bound to the surface of AuNPs measured with thiazole orange (details in the Supporting Information).

(from uncoated AuNPs to 35 bp wtERE-coated AuNPs) in diameter with the DNA shell confirmed that 35 bp dsDNAs are fully extended like a rigid rod on the surface of AuNPs, based on the fact that every 10 bp of a DNA double helix is approximately 3.4 nm in length.[36] In this estimation, the C6 thiol linker is not taken into consideration because its length (0.8 nm) is negligible comparing to the length of the DNA.[37] From zeta potential measurements, dsDNA-AuNPs have slightly reduced negative charges (−32.6 ± 3.4 mV) than the bare AuNPs (−39.2 ± 3.5 mV), as reported previously.[38]

The DNA density determined by using thiazole orange staining method (details in the Supporting Information) was approximately 89.6 ± 5.3 to AuNPs in molar ratio. Despite the slight reduction of surface charge density, DNA conjugated AuNPs is much more stable than bare AuNPs. Particularly dsDNA-AuNPs remained dispersed in NaCl as high as 300 mM as shown by the deep red color and retainable sharp absorption at ∼530 nm (see Figures S2 and S3 in Supporting Information), whereas bare AuNPs have turned into purple at the same salt condition. The enhanced stability against salt screening is another evidence showing that the DNA molecules are successfully conjugated to the particles. The steric protection given by the DNA shell is a more robust stabilizer than the ligand (citrate) coating AuNP.

3.2. Initial Quenching of the Cationic CPEs by dsDNA-Coated AuNPs and Bare AuNPs. Five water-soluble CPEs (3 CCPEs and 2 ACPEs) were involved in this study (Figure 1A). To understand the initial interaction of these CPEs with the negatively charged wtERE-AuNPs conjugates (zeta potential = −32.6 ± 3.4 mV in Table 2), they were mixed (at 100 nM) with dsDNA-AuNPs (50 nM). The fluorescent intensity was measured and compared with the same concentration of CPEs without the NPs (Figure 1B, C). The absorption spectrum of 13 nm AuNPs is given in panels B and C in Figure 1 as a reference to indicate the overlap integral). A lower concentration of 100 nM was used for all CPEs. This concentration was determined after successive experiments with increasing concentration of CPEs. It is well-below the critical concentration of most CPEs, where self-aggregation can lead to a severe drop in fluorescent intensity (i.e., >350 nM for ACPE-560).

For the three CCPEs (Figure 1B), remarkable emission quenching was observed for all of them. FRET from donor (CPEs) to acceptor (AuNPs) is determined by a number of factors, including (1) the distance between donor and acceptor, (2) the relative orientation of donor and acceptor dipole moment, (3) quantum yield of CPE, and (4) the spectral overlap between donor emission spectrum and acceptor absorption spectrum. Assuming the first two factors do not differ much among the three CPEs because of the flexibility of CPEs and the substantial electrostatic interactions, the efficiency of FRET would be mainly governed by the quantum yield and spectral overlap.

In the following discussion, we will attempt to calculate the relative FRET efficiency by considering both quantum yield and spectral overlap. Instead of using the absolute value for quantum yield, we would like to introduce the term` relative fluorescence yield, *f*. We define the relative fluorescence yield as fluorescence intensity of particular CPEs relative to fluorescence intensity of standard (CCPE-630) measured at the same concentration and experimental setup. Because no absolute value was used for the quantum yield, the calculated quenching by FRET is more properly labeled as relative quenching. For the two CCPEs that emit at the blue region of AuNP's absorbance, i.e., CCPE-410 and CCPE-470, the emission intensity is quenched up to 85 and 94% by the dsDNA-AuNPs, respectively. The CCPE-630, which has emission spectrum at the red region of AuNP's absorbance, is only partially quenched (close to 31%). The relative degree of quenching is calculated by multiplying the relative fluorescence yield with spectral integral (*fJ* in Table 3), which is part of formula in calculating the efficiency of FRET. It is found that larger *fJ* values correspond to larger degrees of quenching for the three CCPEs, which validates the assumption that dipole orientation and distance to AuNPs do not differ significantly among the tested CPEs.

For the three CCPEs, because they exhibit opposite charges to the dsDNA-AuNPs, the electrostatic force between them draws CPEs closer to AuNPs. The interaction between CCPEs and AuNPs leads to energy transfer, which results in the nonradiative decay, thus quenching. Although the molecular structure and average molecular weight of each CPE may play a role in controlling their interaction with AuNPs, these factors might have smaller contribution. In the test with bare AuNPs without the dsDNA shell, same quenching trend is observed among the three CCPEs, i.e., CCPE-630 (40%) < CCPE-410 (95%) < CCPE-470 (∼100%), but the degree of quenching is slightly larger than that by the dsDNA-AuNPs. This can be attributed to the removal of dsDNAs molecular barrier that sets a limit on how close the CCPEs can approach to AuNPs, and to the increased negative charges of the bare AuNPs that promotes much stronger electronic interactions.

Table 3. Conjugated Polymer Relative Fluorescence Yield (*f*) and Spectral Overlap Integral with AuNP's Absorption Spectra (*J*)

CP's identity	relative emission yield, *f*	absorbance[a]	integrated area[b]	spectral integral (*J*)	*fJ*	relative degree of quenching by dsDNA-AuNPs (%)
CCPE-410	1.02	0.11	260 543	0.785	0.80	85
CCPE-470	1.19	0.135	363 098	1[c]	1.19	94
CCPE-630	1[c]	0.203	425 698	0.443	0.44	31
ACPE-430	1.28	0.096	288 724	0.589	0.75	15
ACPE-560	1.16	0.072	202 151	0.792	0.92	50

[a]Absorbance at λ = 480 nm. [b]Integrated area under the peak of the emission curve excited with λ= 480 nm. [c]The value used as the reference in calculation. Detailed calculation of quantum yields can be found in the Supporting Information.

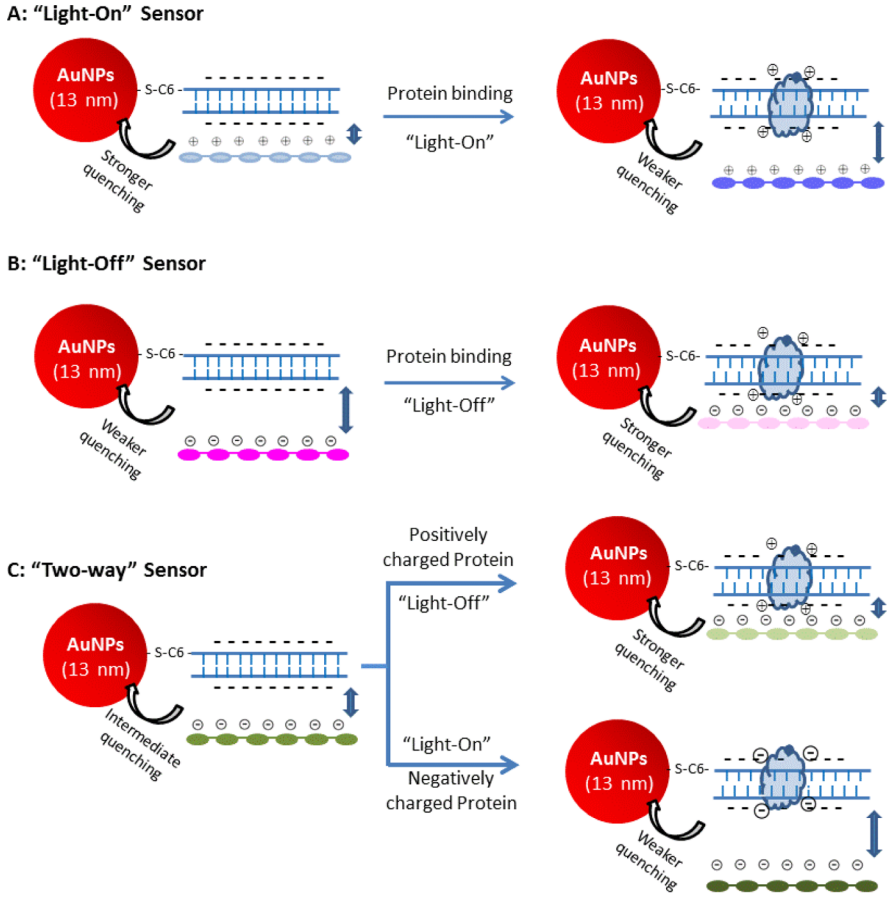

Figure 2. Schematic drawings of (A) "light-on", (B) "light-off", and (C) "two-way" hybrid sensors for detecting protein–DNA binding, according to the degree of initial quenching, i.e., substantial quenching, minor quenching, or intermediate quenching, respectively.

3.3. Initial Quenching of the Anionic CPEs by DNA-Coated AuNPs and Bare AuNPs. For the two anionic CPEs, i.e., ACPE-430 and ACPE-560 (Figure 1C), remarkable quenching (i.e., 15 and 50% of its original intensity) in the presence of dsDNA-AuNPs was observed, but the degree is much smaller relative to that for most of the CCPEs. Despite of same charge of dsDNA-AuNPs entity and ACPEs, and thus charge–charge repulsion, there must be some driving forces that promote the CPEs-AuNPs interaction. We attribute it to hydrophobic interaction between the ACPEs and the dsDNA shell as have been argued by Xu et al.[39,40] As CPEs bear both the polar and nonpolar aromatic and alkyl moieties, the polar side groups assist the solubility in polar solvent. On the contrary, the nonpolar main chains do not favor the polar solvent and is in unstable state. As dsDNA backbone made of alternating sugar (deoxyribose) and phosphate groups, it is likely the nonpolar groups from ACPEs and dsDNA can interact, i.e., via $\pi-\pi$ stacking or van der Waals force. The hydrophobic interaction is mostly an entropic effect originating from the disruption of highly dynamic hydrogen bonds between molecules of polar solvents by the nonpolar entities. By staying together, nonpolar molecules reduce the surface area exposed to polar solvents and minimize their disruptive effect. The hydrophobic interactions between ACPE-430 and dsDNA-AuNPs were confirmed by testing the quenching degree in a series solvent of different polarity (see the Supporting Information, Figure S4). Clearly hydrophobic interaction of ACPEs with DNA is weaker than Coulombic attraction experienced by CCPEs with DNA. As the consequence, ACPEs are separated further from dsDNA-AuNP than CCPEs, and thus less quenching efficiency. Similar to the CCPEs where the degree of quenching is associated with the fJ values, the two ACPEs also follow similar fashion (Table 3). This again indicates that both the spectra overlapping and quantum yield of the CPEs play dominant roles in dictating degree of CPEs' quenching. Similar to that for CCPEs, bare AuNPs quench the emission of ACPEs to a larger degree (i.e., 21% ACPE-430 and 63% ACPE-560), compared to dsDNA-AuNPs, presumably because of the absence of DNA barrier.

The dissimilar interaction between ACPEs and CCPEs to dsDNA-AuNP entity helps to explain why ACPE-430 and CCPE-410 pair which have quite similar value of fJ (0.75 and 0.80, respectively), yet they show a very large difference in quenching behavior (15 and 85%, respectively, by dsDNA-AuNPs). For the two CPEs emitting above 530 nm (AuNPs plasmonic peak), i.e., CCPE-630 and ACPE-560, the lower quenching efficiency is due to either the little spectra overlapping (CCPE-630) or negatively charged (ACPE-560). Though ACPE-560 is anionic, the higher spectral overlap with AuNP's absorbance spectra, gives it more pronounced energy transfer than cationic CCPE-630.

3. 4. Elaboration of the Assay Principle of dsDNA-AuNP/CPE Hybrid Sensor for Detecting Protein Binding. The successful design of the protein binding assay using the dsDNA-AuNPs/CPs hybrid assembly was based on the observation that protein binding can largely change the quenching magnitude. As shown by the schematic drawings (Figure 2), depending on the initial quenching, i.e., substantial

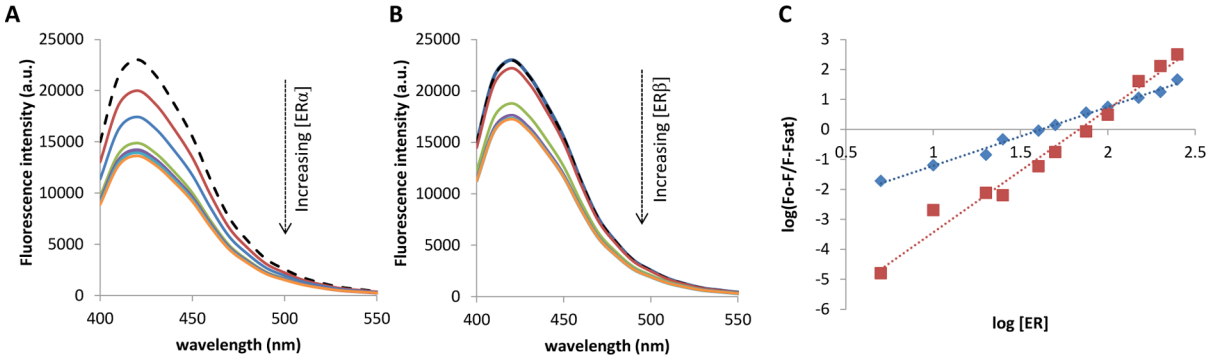

Figure 3. Fluorescence emission spectra of ACPE-430 mixed with wtERE-AuNPs without ER (black dashed line) and with increasing molar concentration of (A) ERα and (B) ERβ relative to DNA (0, 0.5, 1.0, 2.0, 3.0, 4.0, and 5.0 fold). (C) Logarithmic plot of log $[(F_0 - F)/(F - F_{sat})]$ vs log [ERα (diamond) or ERβ (square)] for deducing binding constant (K_d) and binding stoichiometry (see text for more detail).

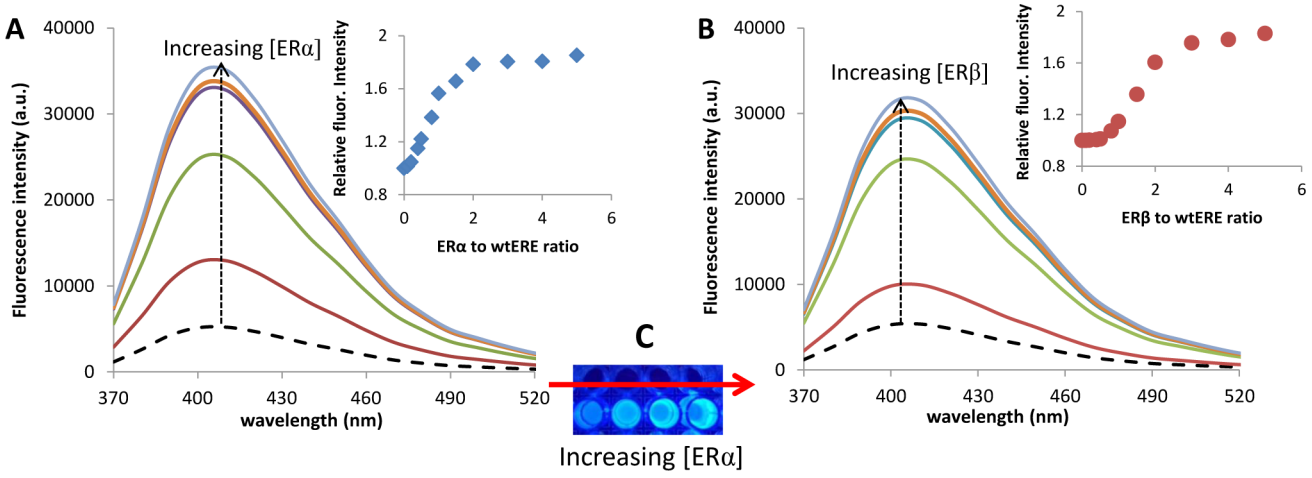

Figure 4. Fluorescence emission spectra of CCPE-410 mixed with ERE-AuNPs without ER (black dashed line) and with increasing molar concentration of (A) ERα and (B) ERβ relative to DNA (0, 0.5, 1.0, 2.0, 3.0, 4.0, and 5.0 fold). The insets summarize change in fluorescence intensity at 410 nm as function of [ER]. (C) Change in fluorescence emission of CCPE-410 as ratio of ERα to ERE is varied from 0, 1, 2, and 5, respectively, under UV light.

quenching (i.e., CCPE-410 and CCPE-470), minor quenching (i.e., ACPE-430), or intermediate quenching (i.e., ACPE-560 and CCPE-630), binding of positively charged protein can be detected by either further enhance the quenching ("light-off" response) or fluorescence restore ("light-on") because protein binding alters the overall charge of the DNA-AuNP, therefore the interaction of CPEs with the particle surface. In the case of intermediate initial quenching, positively and negatively charged protein (or protein with unknown charge properties) can be detected, exploiting "two-way" fluorimetric responses. In the following sessions, "light-on", "light-off", and "two-way" assays were demonstrated for ER-DNA using CCPE-410, ACPE-430, and ACPE-560, respectively. Protein binding not only alters the overall charge of dsDNA-AuNPs entity but also potentially introduces a steric effect that could inhibit hydrophobic interaction of dsDNA-AuNP and CPEs. Therefore, charge and noncharged protein can be detected by this assemble.

3.5. Determination of ERα and ERβ Binding to wtERE-AuNPs with ACPE-430, Exploring Enhanced Quenching, i.e., "Light-off" Principle. Two human ER subtypes, ERα and ERβ, were used to demonstrate the concept. They both are arranged into similar domains and degree of homology varies widely among the regions. Despite the high degree of similarity in the DNA binding domain (96% amino acid identity) and biochemical properties, they differ substantially in tissue distribution. Understanding their distinct DNA binding ability would shed some light if they have differential function and tissue-selective actions.[41] ERα and ERβ (isolectric point, pI ≈ 8.3 and 8.8, respectively)[42] are slightly positive charge at pH 7.4. As demonstrated earlier, ACPE-430 was initially quenched merely by 15% by wtERE-AuNPs (Figure 1C, pink curves). Binding of ERα and ERβ (Figure 3A, B) to wtERE-conjugated AuNPs was evidenced by further drop of the intensity of polymer. We reasoned it as the binding of ER lowers the overall negative charge of DNA-AuNPs (more positive). As a result, more ACPE-430 molecules came closer to AuNPs, resulting in a larger degree of quenching that can be denoted as "light-off" principle. A control experiment was performed to show there is no energy or electron transfer detectable between ACPE-430 and dsDNA or protein (see the Supporting Information, Figure S5).

The distinct binding behavior of ERα and ERβ can be seen qualitatively from the differential protein concentration dependency of ACPE-430 emission (Figures 3 and 4, panels A and B). With the [ER] dependent fluorescence intensity scales, protein–DNA binding affinity constant K_d is calculated quantitatively through $(F_0 - F)/(F - F_{sat}) = ([\text{protein}]/K_d)^n$ (Figure 3C). The K_d was obtained by plotting log $[(F_0 - F)/(F - F_{sat})]$ versus log [protein], where F_0 and F_{sat} are the relative

Table 4. Binding Constant (K_d) of ERα and ERβ with wtERE Measured by Three CPE/DNA-AuNP Hybrid Sensors[a,b]

	ERα		ERβ	
hybrid sensors	K_d (nM)	n	K_d (nM)	n
ACPE-430/dsDNA-AuNPs	42.95 ± 1.85	1.93 ± 0.07	74.09 ± 3.28	4.05 ± 0.13
ACPE-560/dsDNA-AuNPs	41.31 ± 1.54	1.96 ± 0.10	72.90 ± 2.39	4.01 ± 0.23
CCPE-410/dsDNA-AuNPs	45.77 ± 4.89	1.97 ± 0.09	76.04 ± 3.35	3.71 ± 0.19

[a] K_d for ERα-ERE from Sepharose chromatograph is 46 nM [43] [b] ERβ is known to have a two times lower affinity than ERα.[41]

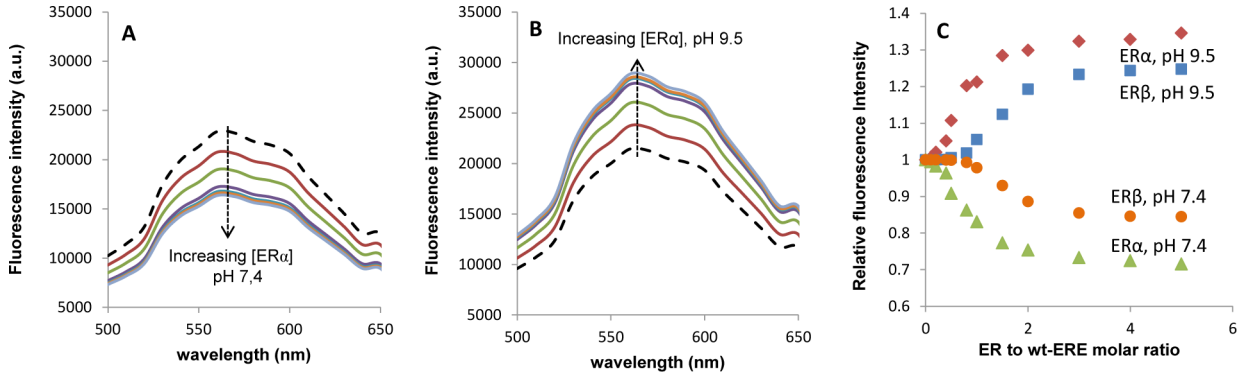

Figure 5. (A, B) Fluorescence emission spectra of ACPE-560 mixed with ERE-AuNPs without ER (black dashed line) and with increasing molar concentration of ERα at (A) pH 7.4 and (B) pH 9.5. (C) The relative change in fluorescent intensity at 560 nm of ACPE-560 as the function of ER concentration for ERα at pH 7.4 (triangle) and pH 9.5 (diamond), and ERβ at pH 7.4 (circle) and pH 9.5 (square).

fluorescence intensities in the absence of protein and in protein saturation respectively. The value of log [protein] at log $[(F_0 - F)/(F - F_{sat})] = 0$ equals to the logarithm of the K_d. The slope, n, is the binding stoichiometry of protein to DNA. The K_d values and stoichiometric (n) values (Table 4) confirm the following characteristics, i.e., ERα binds to wtERE as a dimer (n~2) and more strongly than ERβ ($K_{d,\ ER\alpha} < K_{d,\ ER\beta}$), and ER$\beta$ binds with a ratio of approximately 4 to 1 molar ratio with wtERE as determined previously using SPR spectroscopy.[41] The K_d obtained for ERα correlates well to the value of 46 nM obtained using Sepharose chromatography.[43]

3.6. Determination of ERα and ERβ Binding to ERE-AuNPs with CCPE-410, Exploiting Fluorescence Recovery, i.e., "Light-on" Principle. Although 'light-off' principle works fine in detecting protein binding as has been demonstrated, 'light-on' assay can offer one additional benefit, in which the solution will glow upon protein binding. This is because human eye can quickly adapt to the background illumination and rapidly catch the change in intensity (under UV light) in order to distinguish objects from background.

DNA molecules have net negative charges from the deprotonation of the phosphate group. The addition of CCPE-410, which exhibits opposite charge from DNA, initially produces substantial quenching (i.e., 85% Figure 1A, blue dashed curves). Since ERα and ERβ are positively charged at pH 7.4 ERs binding to ERE will lower the charge of DNA-AuNPs conjugates and thus reduce the electrostatic attraction or the affinity CCPE-410 to AuNP. Thereby fluorescence recovery is expected as the measure of ER-ERE interactions (Figure 4A, B) under the "light-on" principle. This CCPE could be the polymer of choice if visual detection is desirable through the noticeable fluorescence recovery (Figure 4C). Quantitative measurement of ERs affinity with this CCPE-410/AuNPs hybrid sensor gave the same result as the previous ACPE-430 sensor, i.e., ERα has a stronger affinity to wtERE and binds as a dimer than ERβ, which bound as a tetramer.

3.7. Determination of ERα and ERβ Binding to ERE-AuNPs with ACPE-560, Exploiting Both Fluorescence Quenching and Recovery, i.e., "Two-Way" Principle. In previous sessions, we have demonstrated that positively charged proteins can be studied readily with the CCPEs which is either weakly or strongly quenched by dsDNA-AuNPs. Those sensors however, are not suitable to detect negatively charged proteins, due to smaller emission intensity range left to be explored upon negative protein binding. As presented earlier, ACPE-560, although it interacts with DNA through weak hydrophobic interaction that is not favorable of distance-dependent energy transfer, the higher overlap integral between emission of ACPE-560 and absorption spectra of AuNP renders an enhanced quenching to ~50% of the original fluorescence intensity (Figure 1C, green curves). The intermediate fluorescence quenching basically gives ACPE-560 its unique dual-applicability, where it can be used to detect protein binding either by fluorescence quenching or recovery. This "two-way" fashion allows for detecting of proteins of positive or negative charge or proteins on unknown charge properties. To demonstrate the concept ERα was turned into positive and negative by switching the pH of the testing buffer solution between 7.4 and 9.5. At pH 7.4, ERα was positively charged, thus rendered the fluorescence of CP (Figure 5A) being further quenched with its binding to DNA. At pH 9.5, ERα was oppositely charged. The binding to ERE-AuNPs at this pH manifested as the recovery of anionic-560CPE fluorescence intensity (Figure 5B). As the negative ERα bound to DNA, net increase in negative charge of DNA-AuNPs conjugates would repel ACPE-560 further away from the AuNPs surface, hence fluorescence was recovered. Figure 5C is a summary of ER concentration dependent ACPE-560 intensity change at pH 7.4 and 9.5, for ERα and ERβ. K_d values measured for this polymer are reported in Table 4, which is the average values from both methods. They are closely agreed to those measured using the other two CPEs. The close correlation of the K_d values indicate that proper combination charge and emission profiles

(quantum yield and spectral overlap with AuNPs) of CPE, which control the initial degree of quenching, have broaden the simple assay as "light-off", "light-on", or even "two-way" assays that can be tuned to suit different interests. In addition, the consistency of the K_d and n values measured by three CPEs shows the robustness of hybrid sensors. The differential CPEs behaviors, i.e., self-aggregation (if any) and distinct affinity to DNA-AuNPs (if possible) determined by the charge, the chemical structure, and solution pH are not concerns for the hybrid sensor to work. This could be because during the calculation of binding constant and stoichiometry of the protein−DNA interactions, we are measuring the relative fluorescent intensity changes induced by protein binding for a given CPE at a fixed concentration and pH.

3.8. Determination of Binding Energy (affinity) of ERα to Singly Mutated ERE using the CCPE-410 "Light-on" Sensor with a Competition Approach. A perfect ERE contains a palindromic consensus sequence separated by a three-base pair spacer, 5′-GGTCAnnnTGACC-3′. Despite the consensus ERE delineated from conserved cis-regulatory elements found in chicken and *Xenopus Vitellogenin A2* genes, the majority of in vivo EREs deviate from the consensus, with one-half-site identical to that in the consensus and the second half-site having nucleotide variant(s).[44] In a previous study, all possible singly mutated EREs of 15 sequences (3 possible base substitutions at each of 1 to 5 positions from left to right of the 5′ end half site) were created, and dual polarization interferometry (DPI) was used to measure the receptor binding to these mutant EREs to generate an in vitro binding energy model.[30] A motif discovery algorithm, i.e., Thermodynamic Modeling of ChIP-seq (TherMos), was used to compute the binding energy model from in vivo genome-wide ERα binding data. Although the DPI experiment provided a corresponding result with the computational prediction to justify the utility of the in vitro assay for fine study of subtle affinity difference in protein−DNA interactions, there are various hurdles for the equipment intensive DPI assay to become popularized as reliable and convenient tool to understand transcription factor binding in vivo in the whole genome. These technical hurdles include highly technical demanding surface treatment processes (immobilization and regeneration), extensive optimization of fluidic parameters of the solid−liquid phase binding, and the requirement of skillful persona to operate the equipment.

Here, we extended the application of the less equipment intensive hybrid sensors to screen all the singly mutated EREs for their ERα binding, from which we assess the feasibilities (i.e., sensitivity and time required) of this hybrid sensor for detecting subtle affinity difference in large quantity of DNA sequences. Similar to that in DPI solid−liquid phase analysis, a competition approach is used. Using CCPE-410 "light on" sensor as an illustration, the so-called "competition assay" was performed by determine the CCPE-410 emission when ERα binds to wtERE-conjugated AuNPs in the presence of mutant ERE, or "competitors". Depending on the relative affinity of the "competitors" in solution relative to the wtERE on AuNPs surface, the amount of ERα bound to AuNPs and therefore the CCPE-410 emission will be inversely related to the affinity of the competitor DNA. Figure 6A shows the fluorescent intensity plot for ERα binding in the presence of free scrERE, mut12, mut2, or mut7 (mutation signatures please see sequence Table 1) or wtERE as competitor. When the competitor has a weaker affinity to ERα (e.g., the scrERE), more ERα (positively charged at pH 7.4) will be available to bind to wtERE-AuNPs

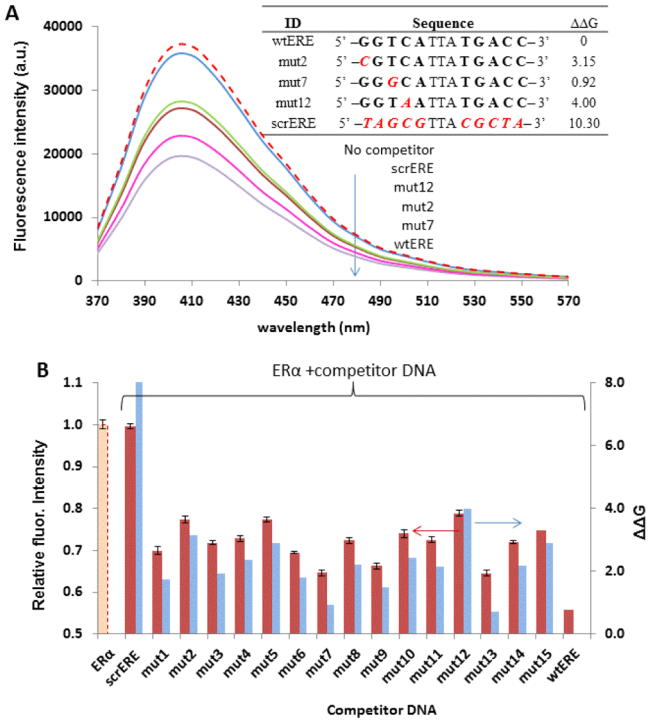

Figure 6. (A) Fluorescence intensity plot of CCPE-410 responding to ERα binding to wtERE-AuNPs in presence of various competitor DNA, i.e., wtERE, scrERE, smut2, smut7, and smut12. The red dashed line refers to emission intensity with ERα binding without any free competitor DNA in solution. (B) Relative fluorescence intensity bar plot for all single mutated EREs as competitor (red bar), with that without competitor DNA as reference (ultra left bar). The blue bars are calculation free energy using TherMos thermodynamic prediction (purple bar[30]).

that leads to stronger repulsion of the CCPE-410 and thus high emission intensity ("light-on"), and vice versa. The intensity trend for all tested competitor (Figure 6A) correlates well with the trend of their free energy value (the larger value the lower affinity), giving the following affinity order wtERE > mut7 > mut2/mut12 > scrERE. For mut12 (the C is replaced by A at position 4), previous gel shift mobility assay suggested that the C to A substitution diminishes the ERα binding due to the steric hindrance between the R211 residue of ERα and nucleotide A.[44] For mut2 (G replaced by C at position 1) it is hypothesized that the weak affinity is due to the electrostatic repulsion between the positively charged reside lysine of the ERα and the positively charge nucleotide C.[45] The same affinity trends has been obtained using the "light-off" ACPE-430 sensor (see the Supporting Information, Figure S6).

When the test was extended for all 15 singly mutant ERE variants, the position- and type-specific affinity trend measured by the DNA-AuNPs/CCPE-410 hybrid sensor correlates very well with the energy matrix derived from the in vivo model using TherMos (Figure 6B). For example, when the hybrid sensor binding bars are similar (e.g., DNA competitors 4, 8, 10, and 11), the corresponding free energy value is also similar. When the hybrid sensor binding bars are higher (i.e., lower affinity of the competitor DNA), the free energy values are also higher. This hybrid sensor generate the following sequence rule, i.e. effect of position and base type specific affinity, at position 1 (G > *T* > A > C), 2 (G > A > *T* > C), 3 (*T* > G > A

> C), 4 (C > T > A ≈ G), and 5 (A > G > T > C), which is consistent with previous report.[45]

The Spearman's rank correlation coefficient[46] (ρ) was calculated between current assay vs Thermos binding energy (ρ1), DPI results vs Thermos binding energy (ρ2) and current assay vs DPI results (ρ3) (the DPI and TherMos data are from reference 28) to assess the significance relation between them. The value was decreasing in this order ρ1 (0.98) > ρ2 (0.91) > ρ3 (0.89). The three correlation coefficient (with degree of freedom =15; 17 samples subtracted by 2) lied above the significance level of 0.1%, which implied that there were 98% chance that the relationship is significant not random. From the correlation coefficient, it was suggested that the CCPE-410/dsDNA-AuNP result corresponds better with the predicted TherMos binding energy, later followed by the DPI results. However, the two sets experimental data (current hybrid sensor and previous DPI) had the lowest similarity (though still considerably related). This could be attributed to the difference in the nature of the two detection assays. Although DPI is a solid−liquid-based detection, where optimized binding conditions are required for protein binding to reach to equilibrium. The nanometer sized CPE/dsDNA-AuNP sensors is considered as a homogeneous phase assay because the substrate (13 nm AuNPs) is in the same size regime as proteins. The high rank correlation of the hybrid sensor versus TherMos, renders the new method highly reliability for understanding of in vivo ERα binding in the whole genome.

4. CONCLUSION

We, for the first time, studied the emission behavior of a series CPEs of different charge properties and emission wavelengths in the presence of DNA-coated gold nanoparticles (AuNPs) under the FRET and/or NSET between the AuNPs acceptor and CPEs donor. Depending on the initial quenching degree, the CPEs/DNA-AuNPs composites can support "light-on", "light-off", and "two-way" detection of sequence specific protein−DNA interactions. Due to the high quenching efficiency between AuNPs and CPEs, the hybrid sensors have a better accuracy and sensitivity in determine binding affinity constant, binding stiochiometry, and single base mutation impact, than sophisticated equipment based methods. The high accuracy, lower equipment dependency, and fast "mix-and-measure" nature make the hybrid sensors promising alternatives for large scale screening protein binding to DNA in the whole genome.

■ ASSOCIATED CONTENT

Supporting Information

Quantification of dsDNA coverage on dsDNA-AuNP conjugates using dye; stability of dsDNA conjugated AuNP; calculation of the quantum yield (Φ) of CPEs; testing the hydrophobic interaction of ACPE-430 and dsDNA, fluorescence of CPEs in the presence of dsDNA or protein, but not AuNPs; determination of binding energy (affinity) of ERα to singly mutated ERE using the ACPE-430 "light-off" sensor with a competition approach. This material is available free of charge via the Internet at http://pubs.acs.org

■ AUTHOR INFORMATION

Corresponding Authors

*E-mail: xd-su@imre.a-star.edu.sg.
*E-mail: cheliub@nus.edu.sg.

Notes

The authors declare no competing financial interest.

■ ACKNOWLEDGMENTS

S.X. acknowledges the Agency for Science, Technology and Research (A*STAR), Singapore for the financial support (JCO 1131CFG001); B.L. thanks Ministry of Defense (R279-000-340-232) for financial support.

■ REFERENCES

(1) Su, S.; Zuo, X . L.; Pan, D.; Pei, H.; Wang, L. H.; Fan, C. H.; Huang, W. *Nanoscale* **2013**, *5*, 2589−2599.
(2) Wang, J.; Qu, X. G. *Nanoscale* **2013**, *5*, 3589−3600.
(3) Liu, B.; Bazan, C. C. *Chem. Mater.* **2004**, *16*, 4467−4475.
(4) Zhu, C.; Liu, L. B.; Yang, Q.; Lv, F.; Wang, S. *Chem. Rev.* **2012**, *112*, 4687−4735.
(5) Feng, X. L.; Liu, L. B.; Wang, S.; Zhu, D. B. *Chem. Soc. Rev.* **2010**, *39*, 2411−2419.
(6) Song, S P.; Qin, Y.; Huang, Q.; Fan, C. H.; Chen, H. Y. *Chem. Soc. Rev.* **2010**, *39*, 4234−424.
(7) Brouard, D.; Viger, M. L.; Bracamonte, A. G.; Boudreau, D. *ACS Nano* **2011**, *3*, 1888−1896.
(8) Li, H.; Wang, A.; Wang, C.; Li, W.; Qiang, W.; Xu, D. K. *Anal. Chem.* **2013**, *85*, 4492−4499.
(9) Han, F.; Guan, Z. P.; Tan, T. S.; Xu, Q. H. *ACS Appl. Mater. Interfaces* **2012**, *4*, 4746−4751.
(10) Polavarapu, L.; Mamidala, V.; Guan, Z. P.; Ji, W.; Xu, Q. H. *Appl. Phys. Lett.* **2012**, *100*, 023106.
(11) Maxwell, D. J.; Taylor, J. R.; Nie, S. *J. Am. Chem. Soc.* **2002**, *124*, 9606−9612.
(12) Jin, Y.; Li, H.; Bai, J. *Anal. Chem.* **2009**, *81*, 5709−5715.
(13) Zhang, J.; Wang, L.; Zhang, H.; Boey, F.; Song, S.; Fan, C. *Small* **2010**, *6*, 3192−3201.
(14) Parker, G. J.; Law, T. L.; Lenoch, F. J.; Bolger, R. E. *J. Biomol. Screening* **2000**, *5*, 77−88.
(15) Li, J.; Huang, Y.; Wang, D.; Song, B.; Li, Z.; Song, S.; Wang, L. H.; Jiang, B.; Zhao, X.; Yan, J.; Liu, R.; He, D.; Fan, C. H. *Chem. Commun.* **2013**, *49*, 3125−3127.
(16) Choi, J. H.; Chen, K. H.; Strano, M. S. *J. Am. Chem. Soc.* **2006**, *128*, 15584−15585.
(17) Levy, M.; Cater, S. F.; Ellington, A. D. *ChemBioChem* **2005**, *6*, 2163−2166.
(18) Han, M.; Gao, X.; Su, J. Z.; Nie, S. *Nat. Biotechnol.* **2001**, *19*, 631−635.
(19) Tang, B.; Cao, L.; Xu, K.; Zhuo, L.; Ge, J.; Li, Q.; Yu, L. *Chem.—Eur. J.* **2008**, *14*, 3637−3644.
(20) Kawasaki, E. S.; Player, A. *Nanomed. Nanotechnol.* **2005**, *1*, 101−109.
(21) Alivisatos, A. P.; Gu, W.; Larabell, C. *Annu. Rev. Biomed. Eng.* **2005**, *7*, 55−76.
(22) Morishita, K.; MacLean, J. L.; Liu, B.; Jiang, H.; Liu, J. W. *Nanoscale* **2013**, *5*, 2840−2849.
(23) De, M.; Rana, S.; Akpinar, H.; Miranda, O. R.; Arvizo, R. R.; Bunz, U. H. F.; Rotello, V. M. *Nat. Chem.* **2009**, *1*, 461−465.
(24) Brouard, D.; Viger, M. L.; Bracamonte, A. G.; Boudreau, D. *ACS Nano* **2011**, *5*, 1888−1896.
(25) Bajaj, A.; Miranda, O. R.; Kim, I. B.; Phillips, R. L.; Jerry, D. J.; Bunz, U. H.; Rotello, V. M. *Proc. Natl. Acad. Sci. U.S.A.* **2009**, *106*, 10912−10916.
(26) Phillips, R. L.; Miranda, O. R.; You, C.; Rotello, V. M.; Bunz, U. H. *Angew. Chem., Int. Ed.* **2008**, *47*, 2590−2594.
(27) Fan, C. H.; Wang, S.; Hong, J. W.; Bazan, G. C.; Plaxco, K. W.; Heeger, A. J. *Proc. Natl. Acad. Sci. U.S.A.* **2003**, *100*, 6297−6301.
(28) Xia, F.; Zuo, X.; Yang, R.; Xiao, Y.; Kang, D.; Vallisle, A.; Gong, X. J.; Yuen, D.; Hsu, B. B.; Heeger, A. J. *Proc. Natl. Acad. Sci. U.S.A.* **2010**, *107*, 10837−10841.
(29) Wang, J.; Liu, B. *Chem. Commun.* **2009**, 2284−2286.

(30) Song, H. Y.; Sun, W.; Prabhakar, S.; Aung, K. M. M.; Su, X. *Anal. Biochem.* **2013**, *433*, 121−128.
(31) Tan, Y. N.; Su, X. D.; Liu, E.; Thomsen, J. S. *Anal. Chem.* **2010**, *82*, 2759−2766.
(32) Tan, Y. N.; Su, X.; Zhu, Y.; Lee, J. Y. *ACS Nano* **2010**, *4*, 5101−5110.
(33) Ou, L. J.; Jin, P. Y.; Chu, X.; Jiang, J. H.; Yu, R. Q. *Anal. Chem.* **2010**, *82*, 6015−6024.
(34) Wang, C.; Zhan, R.; Pu, K. Y.; Liu, B. *Adv. Funct. Mater.* **2010**, *20*, 2597−2604.
(35) Zhang, X.; Servos, M. R.; Liu, J. *J. Am. Chem. Soc.* **2012**, *134*, 7266−7269.
(36) Chatterjee, S.; Lee, J. B.; Valappil, N. V.; Luo, D.; Menon, V. M. *Biomed. Opt. Express* **2011**, *2*, 1727−1733.
(37) Chhabra, R.; Sharma, J.; Wang, H.; Zou, S. L.; Lin, S.; Yan, H.; Lindsay, S.; Liu, Y. *Nanotechnology* **2009**, *20*, 485201.
(38) Seferos, D. S.; Prigodich, A. E.; Giljohann, D. A.; Patel, P. C.; Mirkin, C. A. *Nano Lett.* **2008**, *9*, 308−311.
(39) Xu, Q. H.; Gaylord, B. S.; Wang, S.; Bazan, G. C.; Moses, D.; Heeger, A. J. *Proc. Natl. Acad. Sci. U.S.A.* **2004**, *101*, 11634−11639.
(40) Xu, Q. H.; Wang, S.; Korystov, D.; Mikhailovsky, A.; Bazan, G. C.; Moses, D.; Heeger, A. J. *Proc. Natl. Acad. Sci. U.S.A.* **2005**, *102*, 530−535.
(41) Su, X.; Lin, C. Y.; O'Shea, S. J.; Teh, H. F.; Peh, W. Y.; Thomsen, J. S. *Anal. Chem.* **2006**, *78*, 5552−5558.
(42) Hornbeck, P. V.; Kornhauser, J. M.; Tkachev, S.; Zhang, B.; Skrzypek, E.; Murray, B.; Latham, V.; Sullivan, M. *Nucleic Acids Res.* **2011**, *40*, D261−70.
(43) Bond, J. P.; Notides, A. C. *Anal. Biochem.* **1987**, *163*, 385−390.
(44) Klinge, C. M. *Nucleic Acids Res.* **2001**, *29*, 2905−2919.
(45) Nguyen, D.; Bail, M.; Pesant, G.; Dupont, V. N.; Rouault, É.; Deschênes, J.; Rocha, W.; Melanèon, G.; Steinberg, S. V.; Mader, S. *Nucleic Acids Res.* **2007**, *35*, 3465−3477.
(46) Zar, J. H. Spearman rank correlation. In: Armitage, P, Colton, T, Eds. *Encylopedia for Biostatistics*: Wiley: New York, 2005.